Iranian Journal of Electrical and Electronic Engineering

Journal Homepage: ijeee.iust.ac.ir

# Design of a Novel Barrier-Well Asymmetric Spacer Layer Tunnel Diodes for Implantable Rectenna Circuits

Shamil H. Hussein*(C.A.), and Khalid K. Mohammed**

**Abstract:** This work presents an analysis and design of the two barrier-quantum well asymmetric spacer tunnel layer (QW-ASPAT) diodes for implantable rectenna circuits application. The RF and DC characteristic of a 10×10μm$^2$ QW-ASPAT devices based on GaAs and $In_{0.53}Ga_{0.47}As$ platform was simulated and extracted by using SILVACO atlas software. The highest extracted curvature coefficient, $k_v$ value of the both QW-ASPAT devices at zero bias was about 33V$^{-1}$ compared with the standard structure GaAs/InGaAs was about 13V$^{-1}$. The effects of changing in the thickness of the thin AlAs-barrier, the well width, and the spacer layer are fully investigated on the non-linear relationship between current and voltage of these diodes. A CV simulation was carried out, and it was found that the addition of the quantum-well layer between spacers and barrier reduced the junction capacitance of the QW-ASPAT device when compared with standard devices. The cut-off frequency of the proposed QW-GaAs and QW-InGaAs devices are 26GHz and 46GHz respectively. Finally, we conclude that the QW-ASPAT device is the best structure and can be used for microwave rectifiers in the miniaturized integrated rectenna systems.

**Keywords:** QW-ASPAT Diodes, SILVACO Atlas, and Implantable Rectenna Circuits.

## 1 Introduction

THE Schottky-barrier-diodes (SBDs) is the most common microwave detector diode which has been used since the 1940 [1]. A rectifying/detection diode's need for the capability to production a nonlinear current voltage (I-V) characteristic [2]. The fact that the current transmission mechanism in an SBDs is highly influenced by temperature, it makes it more difficult to employ an SBD in commercial and medical applications. There are several detection devices that portion the similar properties like planar doped barrier (PDB) [3], germanium backward diode (GBD) [4], and the asymmetrical spacer tunnel layers (ASPATs) [5]. The ASPATs is a rectifier high frequency diode that Syme and Kelly initially created in 1992 [6]. It has several advantages such as zero bias voltage operation, insensitivity with temperatures, low noise, and high speed [7]. The ability of lower energy carriers to pass through a higher energy barrier is known as tunneling and is a quantum mechanical phenomenon. As zero bias detector diodes for high frequency applications, tunnel diodes based on QW-InGaAs platforms have been offered for a long time [8]. These diodes have an asymmetrical two un-doped spacers (1, 2) layers thickness of 200:5, quantum well ($t_w$), and the AlAs-barrier ($t_b$) [Monolayers (MLs)] sandwiched between two spacers. So, these devices have asymmetrical I-V characteristics [9]. The figure of merit for any detector or rectifier diode is the curvature coefficient $k_v$ which can be extracted from DC simulation for ASPAT diode. The key $k_v$ of the SBD diode is reached to about 40V$^{-1}$ [10], while the $k_v$ of the Sb tunnelling diode is 47V$^{-1}$ [11], and the Germanium (Ge) based diodes are 70V$^{-1}$ or more [12]. The highest number reported for the $k_v$ of the ASPAT diode are 11 V$^{-1}$ and 10 V$^{-1}$ for standard and proposed devices (GaAs, and InGaAs) respectively [13].

Iranian Journal of Electrical & Electronic Engineering, 2024.
Paper first received 08 December 2022 and accepted 22 August 2024.
* The author is with the Department of Electrical Engineering, University of Mosul, Mosul, Iraq.
E-mail: shamil_alnajjar84@uomosul.edu.iq
** The author is with the Department of Electrical Engineering, University of Mosul, and a dean of Electronic Engineering, Nineveh university, Mosul, Iraq.
Corresponding Author: Shamil H. Hussein.

In this work, a two new devices structure (QW-GaAs and QW-InGaAs) are proposed to increase the $k_v$ to about more than $30V^{-1}$ by adding quantum-well to the thin spacer sides ($S_1$ and $S_2$). The effects of the changing in the thicknesses for the spacers layer, well layer, and thin barrier to the DC and RF characteristics are optimized and simulated by using SILVACO ATLAS. The simulated results and further optimization of the both new structure devices are analyzed and discussed. In addition, it's observed that the current flow through diodes is increased when the mesa size device is increased from $16\mu m^2$ to $100\mu m^2$. The cut off frequency of both $10\times10\mu m^2$ QW-ASPAT devices are 26GHz and 46GHz respectively.

## 2 Physical Modelling of QW-ASPAT Diodes Structures

The two standard ASPATs diode based on GaAs and InGaAs platform was developed on Semi-Insulating (S-I) GaAs. SILVACO ATLAS software is used to design and simulate of the both GaAs/InGaAs devices. The epitaxial layer of the both standard GaAs and InGaAs ASPAT devices are listed in Table 1. The main active area of these diodes consists of a thinner AlAs barrier with thick of 10MLs (2.83nm) that is placed between two un-equal InGaAs spacers by ratio of thick (200nm and 5nm). The curvature coefficient ($k_v$) is one of the key Figure of Merit for any tunnel diode which different its value from design to other and it's represented the second derivative divided to the first derivative of the current voltage (I-V) curve as shown in Eq. (1) below. The highest value of the $k_v$ for both standard ASPAT devices are $13V^{-1}$ and $12.6V^{-1}$ respectively. The conduction-band (C-B) characteristics of a typical ASPAT at different biases is shown in Fig. 1(a). At the AlAs Barrier's base, electrons accumulate and tunnel through it when the bias is in the forward direction. When the bias is reversed, the accumulation layer cannot form because the band-level is not crooked enough, which significantly reduces current flow. In order to increase the factor ($k_v$) at the 0V bias, there must be a substantial difference in current between the forward bias and the reverse bias. One method to widen the gap between two biases in the ASPATs diode is the adding a quantum-well to the narrower spacer sides. Therefore, the new structures of the ASPAT diodes are the QW-GaAs ASPATs and QW-InGaAs ASPATs were proposed. Table 2 describes the epi-layers model of the both proposed QW ASPAT devices. The mesa size area of the QW ASPAT devcie has been used in this work is $10\times10\mu m^2$. In reverse bias, the AlAs barrier height is now higher than in forward bias. Fig. 1(b) shows the conduction bands for both proposed QW ASPAT diodes based on GaAs and InGaAs with 6nm $In_{0.18}Ga_{0.82}As$ and $In_{0.8}Ga_{0.2}As$ quantum well respectively. The C-B profiles of these QW ASPAT devices around the barrier is shown in Fig. 1(c).

The semiconductor-insulator-semiconductor (SIS) model was used to generate the I-V characteristic of the both ASPATs device [14]. This model determines the probability of the transmission by using the Schrodinger equation which can be evaluated by Eq. (2). The variable parameters are the material effective mass (m*), (k) is Boltzmann constant, and (h) is the Planck constant. The fermi-levels ($F_L$) of the spacer layers sandwiched between two side barriers are $E_{Fr}$ and $E_{Fl}$ [15].

$$k_v = \frac{\partial^2 I}{\partial^2 V} / \frac{\partial I}{\partial V} \quad (1)$$

$$J = \frac{q\, m^* kT}{2\,\pi^2 h^3} \int_0^\infty T(E) ln \left\{ \frac{1+e^{\left(\frac{E_{Fr}-E}{kT}\right)}}{1+e^{\left(\frac{E_{Fl}-E}{kT}\right)}} \right\} dE \quad (2)$$

**Table 1** Epitaxial layer structures of the both GaAs and InGaAs standard ASPATs device.

| Thickness [nm] | GaAs - AlAs | | $In_{0.53}Ga_{0.47}As$ - AlAs | |
|---|---|---|---|---|
| | Layers | Doping [cm⁻³] | Layers | Doping [cm⁻³] |
| 300 | GaAs (ohmic 1) | $4\times10^{18}$ | $In_{0.53}Ga_{0.47}As$ (ohmic 1) | $1.5\times10^{19}$ |
| 35 | GaAs (emitter) | $1\times10^{17}$ | $In_{0.53}Ga_{0.47}As$ (emitter) | $1\times10^{17}$ |
| 5 | GaAs (spacer 1) | ---- | $In_{0.53}Ga_{0.47}As$ (spacer 1) | ---- |
| 2.83 | AlAs (barrier) | ---- | AlAs (barrier) | ---- |
| 200 | GaAs (spacer 2) | ---- | $In_{0.53}Ga_{0.47}As$ (spacer 2) | ---- |
| 35 | GaAs (collector) | $1\times10^{17}$ | $In_{0.53}Ga_{0.47}As$ (collector) | $1\times10^{17}$ |
| 350 | GaAs (ohmic 2) | $4\times10^{18}$ | $In_{0.53}Ga_{0.47}As$ (ohmic 2) | $1.5\times10^{19}$ |

**Table 2** Epitaxial layer structures of the both QW-GaAs and QW-InGaAs ASPATs device

| Thickness [nm] | QW- GaAs - AlAs | | QW- $In_{0.53}Ga_{0.47}As$ - AlAs | |
|---|---|---|---|---|
| | Layers | Doping [cm⁻³] | Layers | Doping [cm⁻³] |
| 300 | GaAs (ohmic 1) | $4\times10^{18}$ | $In_{0.53}Ga_{0.47}As$ (ohmic 1) | $1.5\times10^{19}$ |
| 35 | GaAs (emitter) | $1\times10^{17}$ | $In_{0.53}Ga_{0.47}As$ (emitter) | $1\times10^{17}$ |
| 5 | GaAs (spacer 1) | ---- | $In_{0.53}Ga_{0.47}As$ (spacer 1) | ---- |
| 6 | $In_{0.18}Ga_{0.82}As$ well | ---- | $In_{0.8}Ga_{0.2}As$ well | ---- |
| 2.83 | AlAs (barrier) | ---- | AlAs (barrier) | ---- |
| 200 | GaAs (spacer 2) | ---- | $In_{0.53}Ga_{0.47}As$ (spacer 2) | ---- |
| 35 | GaAs (collector) | $1\times10^{17}$ | $In_{0.53}Ga_{0.47}As$ (collector) | $1\times10^{17}$ |
| 350 | GaAs (ohmic 2) | $4\times10^{18}$ | $In_{0.53}Ga_{0.47}As$ (ohmic 2) | $1.5\times10^{19}$ |

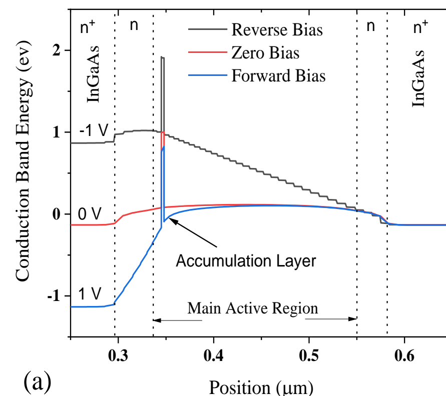

(a)

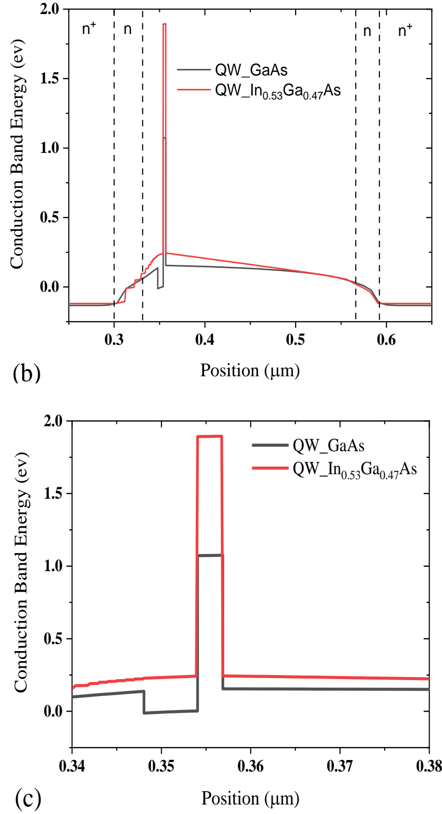


**Fig. 1** Conduction Band (CB) of the typical ASPATs devices with different biases. (b) Zero bais CB profile for both QW-ASPAT diodes, (c) conduction-band profile nearly the barrier-well structure for device in part (b).

SILVACO atlas was used to define the mesh structure model of the QW-InGaAs ASPAT diode which specified seven regions with an epitaxial layer is shown in Fig. 2 for mesa size 10×10μm².

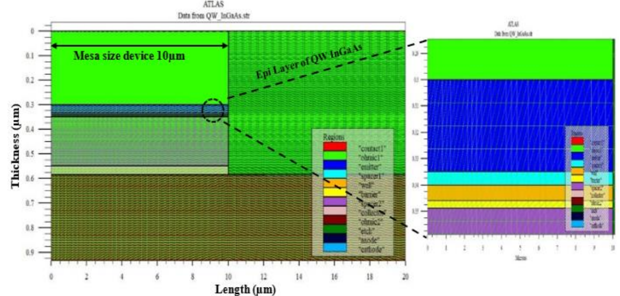


**Fig. 2** Device mesh structure of the new proposed QW-InGaAs ASPAT diode.

## 3 Simulation Results and Discussion

### 3.1 Temperature Dependent Simulation

The impact of temperature variations on the I-V characteristics of ASPAT devices is the main topic of this section. Theoretically, the band-gap, effective mass of electrons, light hole mass, heavy hole mass, permittivity, and mobility of the electron-hole pair are among the various material properties that are impacted by temperature variations. The SBD diode is most commonly used for detector/rectifier circuits, but it has strong sensitivity with temperature which affects to I-V characteristics. The transport mechanism of the charge carriers in SBD by thermionic emission causes high noise. Whereas, the ASPAT diodes the tunneling transport mechanism is dominant due to the height of AlAs barrier being higher compared to SBD.

SBD diodes are most frequently employed in detector/rectifier circuits because of their great temperature sensitivity, which has an impact on their I-V properties. High noise is produced by the thermionic emission technique used in SBD to convey the charge carriers. In contrast, because the AlAs barrier is higher than the SBD barrier, the ASPAT diodes are the tunneling transport mechanism, which is dominant. As a result, ASPAT diodes have a few advantages to SBD such as high speed, low noise, and extremely low temperature sensitivity. Figure 3 shows the temperature sensitivity of SBD and ASPAT diodes. It is evident that the SBD changes are far greater than ASPAT changes.

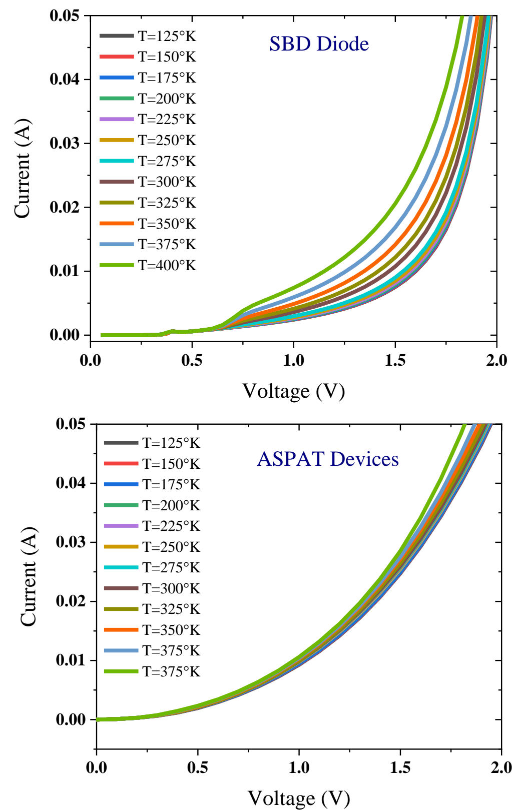


**Fig. 3** The simulated I-V characteristics of SBD and ASPAT diodes as a function of temperatures.

### 3.2 Device DC Characteristics

The DC characteristic of the both standard and new

device ASPATs diodes were simulated for a size device of 10×10μm² using SILVACO ATLAS. From the DC simulation, the I-V characteristic of these devices investigated at 300ºk with a range of bias voltage (-2V to 2V) by 0.01V step changed. Fig. 4(a) shows the IV curve of the proposed diode (QW InGaAs/AlAs-ASPATs) at all mesa size (16μm$^2$, 36μm$^2$, and 100μm$^2$). It's observed at (-2V) of bias input voltage that the current flow through diodes is reduced from (14μA) to (0.9μA) when the mesa size device is decreased from 100μm$^2$ to 16μm$^2$. Therefore, in this paper we take a 10×10μm² size device because it has a high current flow compared with other sizes. As expected, the simulation of the new structures of the ASPAT devices show a leakage current is high reduced compared with conventional ASPAT devices such as GaAs and InGaAs. The QW GaAs based on quantum well $In_{0.18}Ga_{0.82}As$ device having a leakage current of (147 μA) and the QW InGaAs based on $In_{0.8}Ga_{0.2}As$ diode having a current of (14μA) at bias voltage of -2V compared with (1.1mA) and (1mA) for GaAs/InGaAs standard ASPAT devices respectively for same size devices (100μm$^2$). These expected values of the currents on the IV curve for standard and proposed devices have been investigated and simulated. Fig. 4(b) shows the IV characteristic of the GaAs and QW GaAs at zero bias for 100μm$^2$ device.

From the I-V simulated data, the ASPAT devices' critical parameters were extracted. The DC-key parameters ($R_j$ and $k_v$) have been obtained at zero bias-voltage as shown in Fig. 5. It spotted that the highest $k_v$ was extracted at zero bias about 33V$^{-1}$ for both new proposed ASPAT devices compared with standard GaAs diode of 13V$^{-1}$, it is mean that the proposed ASPAT diode is operated as a rectifier / detection correctly. The $R_j$ parameter is increased to much-value about 206kΩ for size device 100μm$^2$ when added quantum well (optimum value of 6nm) to thin barrier layer. Fig. 5(b) shows the extracted junction resistance $R_j$ of the device at bias varied from -2V to 2V. These high values of the $R_j$ are undesirable for the ASPAT devices due to taking large dimensions in the fabrication. Therefore, device optimization is necessary and will be explained in the next section.

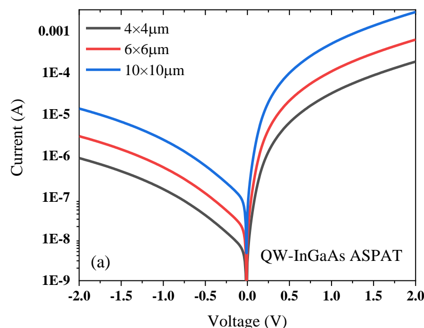


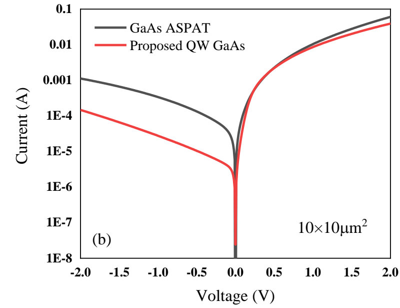


**Fig. 4** (a) The simulated IV characteristic of the proposed QW-InGaAs for all mesa size device, (b) IV curve of the 10×10μm² GaAs and new QW-GaAs.

From the I-V simulated data, the ASPAT devices' critical parameters were extracted. The DC-key parameters ($R_j$ and $k_v$) have been obtained at zero bias-voltage as shown in Fig. 5. It spotted that the highest $k_v$ was extracted at zero bias about 33V$^{-1}$ for both new proposed ASPAT devices compared with standard GaAs diode of 13V$^{-1}$, it is mean that the proposed ASPAT diode is operated as a rectifier / detection correctly. The $R_j$ parameter is increased to much-value about 206kΩ for size device 100μm$^2$ when added quantum well (optimum value of 6nm) to thin barrier layer. Fig. 5(b) shows the extracted junction resistance $R_j$ of the device at bias varied from -2V to 2V. These high values of the $R_j$ are undesirable for the ASPAT devices due to taking large dimensions in the fabrication. Therefore, device optimization is necessary and will be explained in the next section.

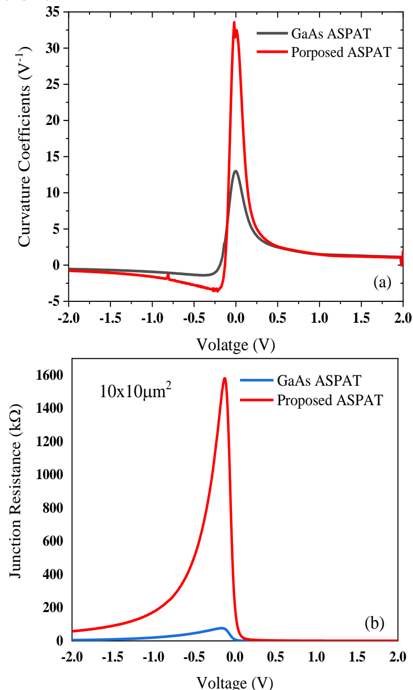


**Fig. 5** (a) The curvature coefficient $k_v$, and (b) the junction resistances $R_j$ extracted for the standard and proposed 100μm² size ASPAT devices.

### 3.3 Device RF Characteristics

SILVACO atlas tool uses to extract the RF characteristic of the both ASPAT devices, the scattering parameters ($S_{11}$) is measured and simulated at room temperature 300ºk. Agilent advanced-design-system (ADS) software has been used to create the circuit model in order to calculate the other key parameters of the ASPAT devices such as junction capacitance, $C_j$ and series resistance $R_s$ [16]. The measurements were taken in steps of 40 MHz from 40 MHz to 40 GHz for frequency and 0.1V step from (-0.6 to 0.6V) for input bias voltage. Fig. 6(a) shows the equivalent circuit model of the ASPATs diode used in this paper. The $S_{11}$ data (Magnitude, and phase value) were simulated for 10×10µm$^2$ of the new device ASPAT as shown in Fig. 6(b). As can be observed from this figure, excellent matches between data simulation from the SILVACO atlas and an equivalent model created by using the s1p block found in the ADS package.

The C-V simulation of the ASPAT didoes has been investigated by using numerical results in SILVACO atlas to obtain the $C_j$ values as a function of bias applied voltage for range (-0.6 to 0.6) V. The $C_j$ is increased when the mesa size device increases under zero and forward biased voltage. The key $C_j$ of the both 100µm$^2$ GaAs and proposed QW-GaAs diodes extracted at zero bias are 180fF and 107fF respectively as shown in Fig. 7 (a). While the $C_j$ of the InGaAs and QW InGaAs devices are 157fF and 65.6fF respectively for the same size area is shown in Fig. 7(b). In the same manner, The $R_s$ of the ASPAT devices increase under zero and forward bias voltage, matching the behavior of calculated $C_j$. This is because the layer of un-doped spacers is not completely depleted. The accumulating region at the device barrier's base increases capacitance when it is biased forward. Fig. 7(c), and (d) describes the $R_s$ value of the both conventional and new structures ASPAT diodes.

The cut off frequencies ($f_c$) and operating frequency ($f_o$) are the most important factor to evaluate working of the tunnel ASPAT devices. These frequencies depended on the $R_s$ and $C_j$ extracted from the RF properties for these diodes. The $f_o$ frequency represents a 1/3 value of the $f_c$. The $f_c$ can be calculated by Eq. (3). The $f_c$ of the both new structure diodes used in this work are 26GHz and 46GHz respectively. Table 3 shows the complete key parameters extracted at zero bias of the all ASPAT devices for the mesa size of 100µm$^2$. This table shows that the QW InGaAs and QW GaAs have higher $f_c$ frequencies than the standard GaAs/InGaAs diodes.

$$f_c = 1/(2 * \pi * R_s * C_j) \quad (3)$$

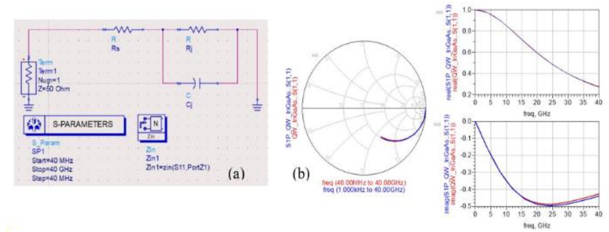


**Fig. 6** (a) The circuit model of ASPATs is made by ADS, (b) S11 parameters of the proposed 100µm2 QW-InGaAs ASPAT device at bias of 0V.

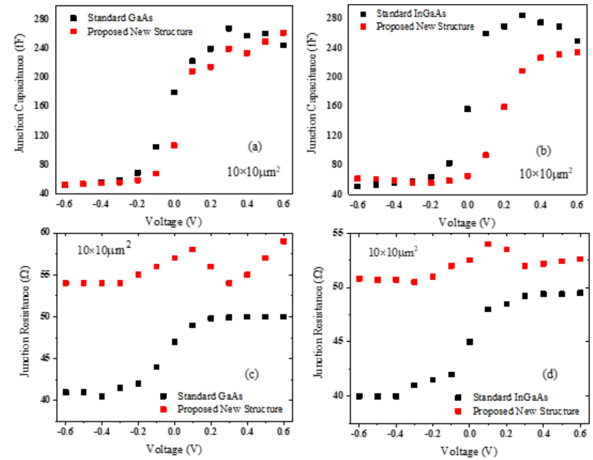


**Fig. 7** (a), (b) Extracted capacitance Cj of the both standard and proposed new 10×10µm2 ASPAT diodes plotted with input voltage. (c), (d) The value of the resistance Rs for the both standard and new structure ASPAT with the same size.

**Table 3** Extracted zero bias parameters for proposed and others ASPAT devices

| ASPAT Device Structure | Mesa Size Device [µm$^2$] | $K_v$ [$V^{-1}$] | $R_j$ [kΩ] | $R_s$ [Ω] | $C_j$ [fF] | $f_c$ [GHz] | $f_o$ [GHz] |
|---|---|---|---|---|---|---|---|
| **Standard GaAs/AlAs** | 4×4 | 13 | 24 | 62 | 34 | 75 | 25 |
| | 6×6 | | 7.12 | 55 | 77 | 38 | 13 |
| | 10×10 | | 1.54 | 47 | 180 | 19 | 6.5 |
| **Standard $In_{0.53}Ga_{0.47}As/AlAs$** | 4×4 | 12.6 | 30.5 | 53 | 22.2 | 135 | 45 |
| | 6×6 | | 9.03 | 50 | 60 | 53 | 18 |
| | 10×10 | | 1.95 | 45 | 157 | 23 | 7.5 |
| **Proposed New structure QW-GaAs/AlAs (GaAs/AlAs with 6nm $In_{0.18}Ga_{0.82}As$ quantum well)** | 4×4 | 32.5 | 126 | 65 | 17.2 | 143 | 47 |
| | 6×6 | | 22.4 | 56 | 39 | 73 | 25 |
| | 10×10 | | 8.07 | 57 | 107 | 26 | 9 |
| **Proposed New structure QW-InGaAs/AlAs ($In_{0.53}Ga_{0.47}As$ with 6nm $In_{0.8}Ga_{0.2}As$ quantum well)** | 4×4 | 33 | 3170 | 50 | 10.5 | 303 | 101 |
| | 6×6 | | 946 | 52 | 23.4 | 130 | 44 |
| | 10×10 | | 206 | 52.5 | 65.6 | 46 | 15 |

## 4 QW ASPAT Device Optimization and Discussions

In this section, we describe the effect for both of the thin AlAs barrier thickness (MLs), the spacers side layer ($S_1$ and $S_2$) in nm, and the quantum well thickness to both characteristics (RF, and DC) of the ASPAT diodes. Firstly, the barrier thickness ($t_b$) of the both QW-ASPAT tunnel diodes has an exponentially impact on the electron tunneling through it, this effect leads to make the I-V Characteristic show asymmetric-behavior, forward and reverse current rise by two orders of magnitude. Fig. 8(a) shows the effect $t_b$ to the

characteristic of the proposed QW-GaAs ASPAT diode when the mesa size device of 100µm$^2$ and the spacer 1, 2 ($S_1$, and $S_2$) are 5nm and 200nm respectively. Fig. 8(b) explain the effect $t_b$ to the proposed QW-InGaAs ASPAT diode characteristic. Thus, the optimum value of the thick ($t_b$) has been selected in this work is 10MLs (2.83nm) and reported in table 2.

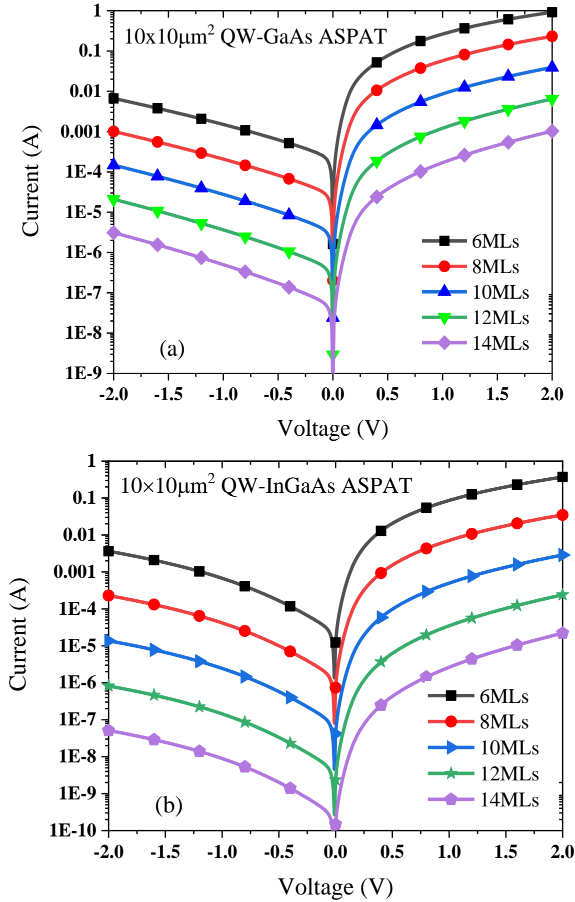


**Fig. 8** Current and voltage (I-V) curve of the proposed, (a) QW-GaAs ASPAT and (b) QW-InGaAs ASPAT device for same size area when the thickness of the barrier ($t_b$) is changed.

The thickness of the spacer 1 and 2 ($S_1$, $S_2$) for the proposed structure ASPAT diode are 5nm, and 200nm respectively. Now, we study the full impact of each thickness individually on the diode performances at zero bias such as IV curve. For thick-barrier ($t_b$) 10MLs, the thickness ($S_1$) and ($S_2$) are changed from 5 to 30nm and 50-225nm respectively. Fig. 9 (a), and (b) show the QW-GaAs ASPATs I-V curve with varying spacers 1, 2 thickness respectively. The current in forward bias is unchanged by an increase in $S_2$ for a constant value of $S_1$, while in reverse bias the current is decreased because of a further increase in the voltage drop within the thick spacer layer. As results, the current is decreased in the reverse bias. For $S_1$ varying from 5 nm to 30 nm and $S_2$ fixed at 200 nm, different behavior is observed. For instance, it was found that as $S_1$ increases thicker under forward and reverse bias values, due to an increase in the voltage drop driven on by the same spacer, the simulated current is reducing. Fig. 9 (c), and Fig. 9 (d) show the VI curve of the new device QW InGaAs ASPAT when changing spacer sides ($S_1$) and ($S_2$) respectively.

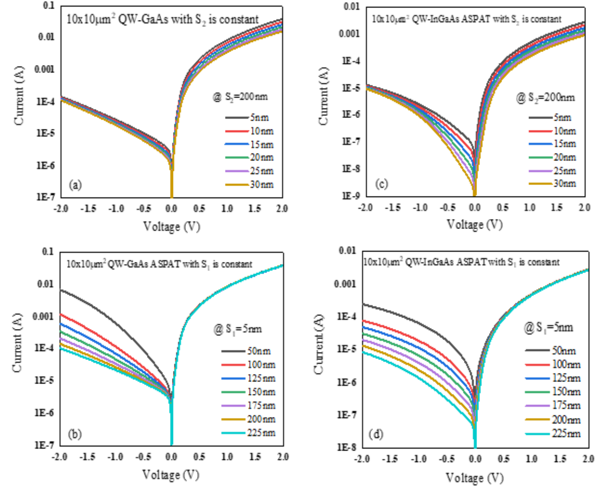


**Fig. 9** The current-voltage (IV) curve of a new device QW-GaAs ASPATs diode, when the spacer ($S_1$) in (a) and the spacer ($S_2$) in (b) are changed. The new diode QW-InGaAs ASPAT devices in (c) and (d) for the same spacer change ($S_1$) and ($S_2$) respectively. All remaining other parameters are constants as reported in table 2.

In order to reduce the value of $R_j$ which appeared in the new structures of the both proposed QW-ASPAT devices. The effect of the well thick($t_w$) and the thin-barrier thickness on the both ($R_j$) and ($k_v$) were simulated and varied from (2nm to 8nm) and (6MLs to 14MLs) respectively. From these simulations, $R_j$ and $k_v$ at zero bias were taken out and utilized to make a map of all potential combinations as shown in Fig. 10 for both QW-ASPAT diodes. It is observed that reducing the well ($t_w$) causes the junction resistance to decrease. The $k_v$ is also reduced as a result, though. These simulations' outcomes show that the resistance ($R_j$) and thickness ($t_b$) have a significant exponential relationship. It is demonstrable that by decreasing the ($t_b$) from 14MLs to 6MLs, $R_j$ decreased from 540kΩ to 0.12kΩ for QW-GaAs device, and from 57GΩ to 0.7kΩ for QW-InGaAs with the $t_w$ of 6nm. These values of the $R_j$ are more appropriate for diode rectifier applications.

For the new device QW-GaAs, the highest value of $k_v$ was about 34V$^{-1}$, while for the QW-InGaAs structure was 33V$^{-1}$. The most important method of reducing the $R_j$ values is to decrease the $t_b$ without significantly reducing $k_v$, as observed from Fig. 10. Therefore, the value of the $k_v$ and $R_j$ have been selected are 33V$^{-1}$ and 206kΩ respectively for QW-InGaAs diode.

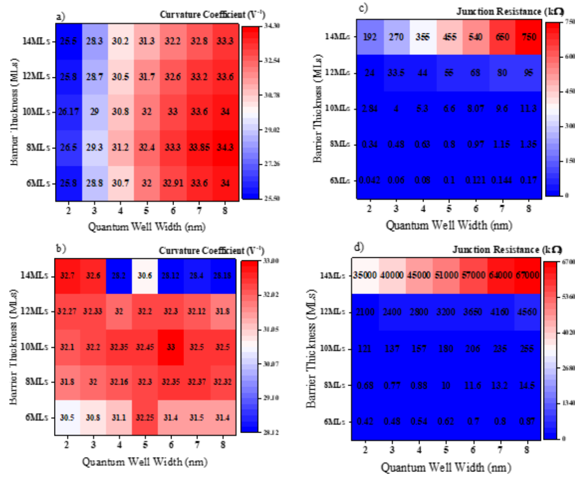


**Fig. 10** (a), (b) Extracted kv values for simulations of the QW-GaAs and QW-InGaAs devices respectively when changing both the well and barrier thicknesses. (c), (d) Extracted Rj values of the same diodes in (a) and (b) by varying the quantum well from 2nm to 8nm.

## 5 Implantable Rectenna Circuit Design

To satisfy the increasing requirements of end users in the fields of industrial and healthcare monitoring, interest in wireless sensor networks and implanted devices has recently become popular [17]. The overall size area, power consumption, and meeting medical treatment requirements of the devices are factors to take into account when it's implanted in-body [18]. The final dimensions of the chip can be implanted to a scale of less than 10mm$^2$ through minimally invasive therapy and the polarization-free detector greatly reduces the power dissipated of the circuit [19]. Therefore, the fully integrated rectenna circuit was used for implanted medical devices. The miniaturized rectenna system consisting of high nonlinearity and temperature insensitivity ASPAT diodes were used in the rectifying circuits and integrated with a planar dipole antenna for operating at dual band ISM frequency (1.5GHz and 5.8GHz).

In this work, the 100µm$^2$ (QW-ASPAT) was used as a rectifier diode in the rectifying circuit which integrated with the implantable dual folded dipole antenna (FDA) to build rectenna circuits. The FDA was analyzed and designed by numerical simulation in the Computer Simulation Technology (CST) microwave studio software [20]. Two symmetrical radiating arms with various L-shaped conducting sections made up the FDA antenna. Fig. 11 show a 1×4.5mm$^2$ FDA designed to resonate at the 1.5GHz and 5.8GHz. All the optimized parameters are marked in Fig. 11 and detailed in table 4. The radiating planar structure is mounted on a high-permittivity dielectric substrate (Gallium arsenide, $\varepsilon_r$=12.94, tanδ=0.006) of 0.63mm thick semi-insulating GaAs substrate ($h_s$) and covered with an identical glue ($h_{glue}$) and superstrate ($h_{super}$) layer. In addition, a non-uniform metal strip widths of the main and secondary arm (w and t) were used along the antenna structure varying from 0.01 to 0.07mm in order to enhance effective antenna dimensions. The $Z_{in}(real)$ and $Z_{in}(imaginary)$ component of the antenna can be influenced by changes in (w and t), respectively. Additionally, the folded-arm technique shows reduced dimensions of the antenna structure, and the $L_1$ to $L_9$ lengths can be used to find the resonance frequency.

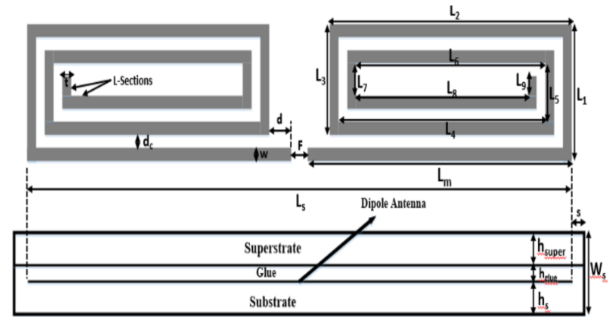


**Fig. 11** Geometry of the 1×4.5mm2 implantable FDA antenna structure with main and secondary L-section arms.

**Table 4** The folded dipole antenna's optimized parameters

| Parameters | Value [mm] | Parameters | Value [mm] |
|---|---|---|---|
| $L_s$ | 4.5 | $L_8$ | 1.825 |
| $W_s$ | 1 | $L_9$ | 0.3 |
| $L_m$ | 2.15 | F | 0.1 |
| $L_1$ | 0.9 | s | 0.05 |
| $L_2$ | 2.125 | d | 0.075 |
| $L_3$ | 0.8 | $d_c$ | 0.05 |
| $L_4$ | 2.025 | w = t | 0.05 |
| $L_5$ | 0.7 | $h_s = h_{super}$ | 0.63 |
| $L_6$ | 1.925 | $h_{glue}$ | 0.05 |
| $L_7$ | 0.9 | $h_c$ | 0.001 |

The overall size of the proposed antenna is 2.835 mm$^3$ (1×4.5×0.63) mm$^3$. The reflection coefficient ($S_{11}$) of the dual-band FDA antenna is shown in Fig. 12. The antenna exhibits a simulated 10-dB impedance bandwidths in a 4-layer phantom at 1.5GHz and 5.8GHz are 227MHz (1.4-1.63GHz) with $S_{11}$ is -22.6dB and 540MHz (5.47-6.02GHz) with $S_{11}$ is -23.1dB respectively. Due to low gain and efficiency of the antenna, the voltage doubler rectifier (VDR) circuit was used which consists of two tunnel diodes $D_1$ and $D_2$ (100µm$^2$ QW-ASPAT) and input/output filters. The proposed full rectenna circuit as shown in Fig. 13

consists of received FDA antenna, VDR rectifier circuit, and the load resistance ($R_L$).

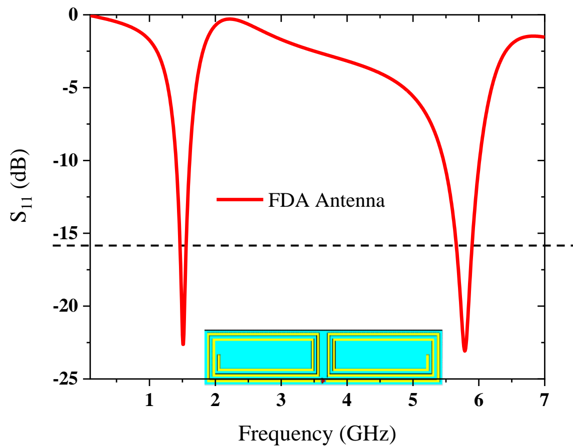


**Fig. 12** Reflection coefficient $S_{11}$ characteristics of the implantable dual FDA antenna.

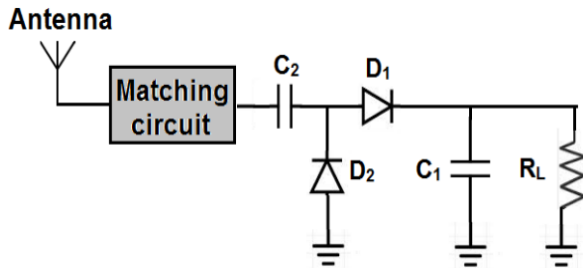


**Fig. 13** The schematic of the full rectenna circuit design.

The impedance $Z_{in(QW-InGaAs)}$ of the 100μm$^2$ size device are (65-j*1620) Ω and (53-j*418) Ω for dual band 1.5GHz and 5.8GHz respectively. In order to achieve perfect matching between QW-ASPAT diode and antenna, we must calculate the input impedance of the VDR circuit $Z_{in(VDR)}$ that contains the QW-ASPAT diodes ($D_1$ and $D_2$). The $Z_{in(VDR)}$ for proposed dual bands are (56-j*915) Ω and (58-j*236) Ω respectively at input power of the antenna is 10dBm. It observed from results that the real part impedance of the antenna and VDR circuit are matched compared with different imaginary parts. The reactance part can be cancelled by adding an input matching network which is constructed on the ADS library. Fig. 14 shows the return loss at dual bands of the matching response between the planar 1×4.5mm$^2$ dipole antenna and the QW-InGaAs ASPAT diode. The rectenna circuit exhibited reasonable matching performance at an input RF power (Pin) of 0dBm as well.

The DC output voltage is acquired by the optimum $R_L$ and $C_L$. The optimized values of the $R_L$ are 1.7kΩ and 0.5kΩ for 1.5GHz and 5.8GHz respectively. Of course, a higher $R_L$ results in a higher output voltage. The voltage which is provided from the implantable rectenna circuit is used to wireless power transfer to implantable medical devices inside the human arm model. Fig. 15 shows the voltage ($V_{out}$) and power ($P_{out}$) of the full rectenna model by using single and double stage of the VDR circuit at optimum $R_L$ of 0.5kΩ. It is clear that the voltage and power were about (0.8V and 1.6V) and (34μW and 68μW) for the single and double stage of the VDR respectively at frequency of 5.8GHz and Pin of 10dBm.

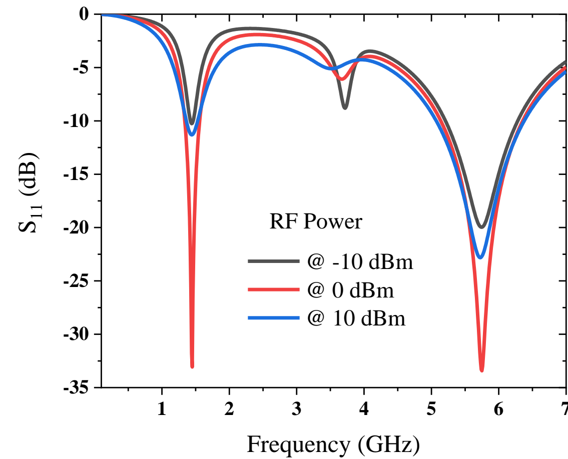


**Fig. 14** The Return loss of the implantable proposed rectenna circuit model.

The RF to DC conversion efficiency (η) of the full rectenna system as a function of RL was calculated from the ratio (PDC / Pin) as shown in Fig. 16(a). The circuit has a η of 4.4% at an optimum load of 1.7kΩ for frequency of 1.5GHz, and 16.5% for resonance frequency of 5.8GHz with optimum RL is 0.5kΩ. The power conversion efficiency (PCE %) of the proposed dual-band rectenna system has a maximum value about (75%) and (93%) at the optimum load resistor for 1.5GHz and 5.8GHz respectively, as shown in Fig. 16(b). These results lead to that the rectenna circuit operated correctly at the optimized load and the resonance frequency bands.

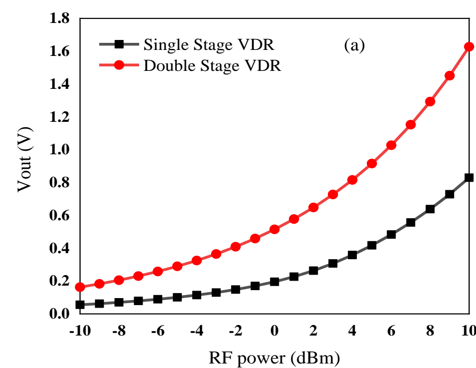

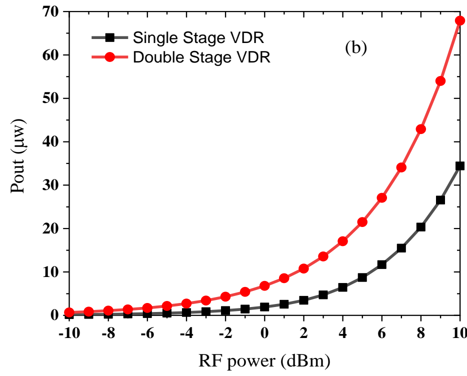


**Fig. 15** The DC output voltage and power of the rectenna circuit with single and double stage VDR circuit at frequency of 5.8GHz for (a), and (b) respectively.

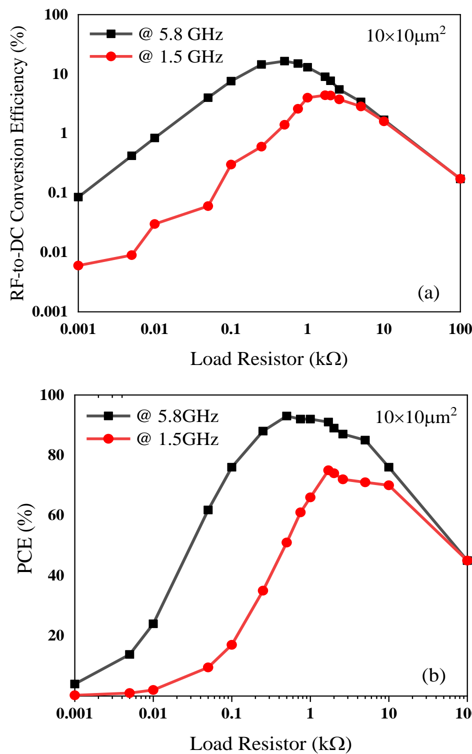


**Fig. 16** (a) The RF to DC conversion efficiency (η) of the full rectenna system, (b) Power conversion efficiency (PCE%) of the dual-band implant rectenna circuit with the size of 100µm2 QW-ASPAT diode.

In this work, dual band implantable rectenna system design for biomedical applications requires miniaturization and is biocompatible with human's tissues. Table 5 shows the performance comparison of the proposed dual-band implantable rectenna circuit with literature. It is observed and concluded from this table that the rectenna circuit has very small size area, low cost and the better results obtained for operation in dual-band resonance frequency.

**Table 5** Performance comparison of the proposed implantable rectenna system with literature

| Ref/ year | Antenna / rectifier topology | Freq. bands [GHz] | Device Size [mm³] | Gain [dBi] | Pt/Pr [Watt] | Rectenna Efficiency [%] |
|---|---|---|---|---|---|---|
| [21] | Spiral structure with T-shaped ground slot / HWR single diode | 0.402<br>1.4<br>2.45 | 11×26×1.6 | -31 | 0.5/125µ | 2.5 |
| [22] | Folded with stubs / CMOS full-wave rectifier circuit | 5.8 | 3×1.5×1.6 | -29.5 | 4/16.6µ | --- |
| [23] | Foded dipole antenna / VDR with conventional ASPAT | 2.45 | 1×5×0.625 | -26.9 | 0.1/16.4µ | 1.2 |
| [24] | Foded dipole with stubs/VDR based on GaAs ASPAT diode | 2.35 | 1.2×4×0.6 | -24.7 | 0.1/19.6µ | 2 |
| This Work | Foded dipole antenna / VDR with proposed ASPAT diodes | 1.5 | 4.5×1×0.63 | -36.9 | 0.1/167µ | 4.4 |
| | | 5.8 | | -24.4 | 0.1/45µ | 16.5 |

## 6 Conclusion

The two new quantum well-barrier (QW-ASPAT) diodes design have been proposed in this paper to enhance the value of the curvature coefficient, $k_v$ of the ASPAT devices. The standard and new structures have been simulated and modelled physically by using SILVACO atlas software. The highest $k_v$ value at zero bias of the QW-ASPATs device was $32.6V^{-1}$ and $33V^{-1}$ for GaAs and InGaAs based structures respectively compared with $12.6V^{-1}$ and $13V^{-1}$ for standard GaAs and InGaAs. To increase the value of resistance ($R_j$), the effect of changing the thickness of the thin AlAs-barrier, well width, and spacers layer thickness on the nonlinear relationship between current and voltage of the ASPATs diodes were comprehensively investigated. Rj was observed to be exponentially proportional to barrier thickness and proportionate to well thickness.

The insertion of quantum well to the thinner spacer on the ASPAT device at zero bias, decreases the value of capacitance $C_j$ from 180fF to 107fF and from 157fF to 65.6fF for QW-GaAs and QW-InGaAs respectively, compared with standard ASPAT devices. The cut off frequency of the both proposed 10×10µm² QW-ASPAT devices are 26GHz and 46GHz respectively. The proposed diodes have been used as a rectifying circuit which integrated with dual band FDA antenna to build the rectenna system. The rectenna circuit converts RF power to DC voltage for charging medical devices inside the human body. The VDR circuit was used as a single and double stage, the DC output voltage and power of the rectenna for double stage rectifiers are twice that produced by the single stage at the input RF power of 10dBm. The maximum conversion efficiency (η) of the full proposed rectenna system has been obtained at dual-

bands resonance frequency when the load resistance integrated was optimum.

## Conflict of Interest

The authors declare no conflict of interest.

## Author Contributions

Shamil Alnajjar: Conceptualization, Methodology, Software, Formal analysis, Writing - Original draft. Assist. Prof. Dr. Khalid K. Mohammed: Supervision, Revise & editing, Investigation.


## Funding

No funding was received for this work.


## Informed Consent Statement

Not applicable.

## References


[1] T. Shimaoka, S. Koizumi, JH, and Kaneko, "Recent progress in diamond radiation detectors," *Functional Diamond*, vol. 1, no. 1, pp. 205–220, 2022.

[2] J. Wang, M. Naftaly, and E. Wasige, "An Overview of Terahertz Imaging with Resonant Tunneling Diodes," *Applied Sciences*, vol. 12, no. 8, p. 3822, 2022.

[3] M. J. Akura, "Simulation of semiconductor devices: the Potential Well Barrier and Planar-doped Potential-Well Barrier diodes," 2020.

[4] I. I. Izhnin *et al.*, "Single-photon avalanche diode detectors based on group IV materials," *Applied Nanoscience*, pp. 1–11, 2021.

[5] K. Z. Ariffin *et al.*, "Asymmetric spacer layer tunnel diode (ASPAT), quantum structure design linked to current-voltage characteristics: A physical simulation study," presented at the 2017 10th UK-Europe-China Workshop on Millimetre Waves and Terahertz Technologies (UCMMT), 2017, pp. 1–4.

[6] K. N. Z. Ariffin, *Physical Modelling of Tunnel Diodes for Terahertz Frequency Applications*. The University of Manchester (United Kingdom), 2019.

[7] A. J. Hadfield, "Heterostructure Tunnel Diodes for Terahertz and mm-Wave applications," 2021.

[8] O. S. H. Abdulwahid, *Advanced Quantum Mechanical Tunnelling Based Devices and Avalanche Breakdown Photodiodes for Radio Frequency and Optical Detection Systems*. The University of Manchester (United Kingdom), 2019.

[9] A. Hadfield, A. Salhi, J. Sexton, and M. Missous, "Experimentally Validated Physical Modelling of Asymmetric Spacer Layer Tunnel Diodes for THz Applications," presented at the 2019 12th UK-Europe-China Workshop on Millimeter Waves and Terahertz Technologies (UCMMT), 2019, pp. 1–3.

[10] A. S. Hajo, O. Yilmazoglu, F. Küppers, and T. Kusserow, "Integration and characterisation of Schottky diodes with a pre-amplifier for THz applications," presented at the 2020 45th International Conference on Infrared, Millimeter, and Terahertz Waves (IRMMW-THz), 2020, pp. 1–2.

[11] F. Rothmayr *et al.*, "Mid-infrared GaSb-based resonant tunneling diode photodetectors for gas sensing applications," *Applied Physics Letters*, vol. 112, no. 16, p. 161107, 2018.

[12] A. Hadfield, A. Salhi, J. Sexton, and M. Missous, "Novel barrier-well heterostructure diodes for microwave and mm-wave applications," *Solid-State Electronics*, vol. 178, p. 107963, 2021.

[13] O. Abdulwahid, S. G. Muttlak, J. Sexton, M. Missous, and M. Kelly, "24ghz zero-bias asymmetrical spacer layer tunnel diode detectors," presented at the 2019 12th UK-Europe-China Workshop on Millimeter Waves and Terahertz Technologies (UCMMT), 2019, pp. 1–3.

[14] N. Tuomisto, A. Zugarramurdi, and M. J. Puska, "Modeling of electron tunneling through a tilted potential barrier," *Journal of Applied Physics*, vol. 121, no. 13, p. 134304, 2017.

[15] A. Salhi, J. Sexton, S. Muttlak, O. Abdulwahid, A. Hadfield, and M. Missous, "InGaAs/AlAs/GaAs metamorphic asymmetric spacer layer tunnel (mASPAT) diodes for microwaves and millimeter-waves detection," *Journal of Applied Physics*, vol. 127, no. 19, p. 194505, 2020.

[16] A. A. ISMAEL, A. T. YOUNIS, E. A. ABDO, and S. H. HUSSEIN, "IMPROVEMENT OF NON-LINEAR POWER AMPLIFIER PERFORMANCE USING DOHERTY TECHNIQUE," *Journal of Engineering Science and Technology*, vol. 16, no. 6, pp. 4481–4493, 2021.

[17] M. Kumar, "Social, economic, and environmental impacts of renewable energy resources," *Wind Solar Hybrid Renewable Energy System*, vol. 1, 2020.

[18] M. M. H. Shuvo, T. Titirsha, N. Amin, and S. K. Islam, "Energy Harvesting in Implantable and Wearable Medical Devices for Enduring Precision Healthcare," *Energies*, vol. 15, no. 20, p. 7495, 2022.

[19] S. G. Muttlak, M. Sadeghi, K. Ian, and M. Missous, "Low-Cost Compact Integrated Rectenna for Implantable Medical Receivers," *IEEE Sensors Journal*, vol. 22, no. 17, pp. 16938–16944, 2022.

[20] S. G. Muttlak, M. Sadeghi, K. Ian, and M. Missous, "Miniaturized Folded Antenna with Improved Matching Characteristic for mm-wave Detections," presented at the 2021 14th UK-

Europe-China Workshop on Millimetre-Waves and Terahertz Technologies (UCMMT), 2021, pp. 1–3.

[21] Das, Rupam, and Hyoungsuk Yoo. "A multiband antenna associating wireless monitoring and nonleaky wireless power transfer system for biomedical implants." IEEE Transactions on Microwave Theory and Techniques 65.7 (2017): 2485-2495.

[22] Radiom, Soheil, et al. "Far-Field On-Chip Antennas Monolithically Integrated in a Wireless-Powered 5.8-GHz Downlink/UWB Uplink RFID Tag in 0.18-µm Standard CMOS." IEEE Journal of Solid-State Circuits 45.9 (2010): 1746-1758.

[23] Muttlak, Saad G., et al. "Low-Cost Compact Integrated Rectenna for Implantable Medal Receivers." IEEE SENSORS JOURNAL 22.17 (2022): 16938-16944.

[24] Walsh, Christopher, et al. "Miniature Integrated 2.4 GHz Rectennas Using Novel Tunnel Diodes." *Sensors* 23.14 (2023): 6409.

Shamil H. Hussein Alnajjar was born in 1984 in Mosul / Iraq, he received the B.Sc. degree from the University of Mosul / Electrical Engineering Department at electronic & communication. He finished his M.Sc. in Electronics from Mosul University / Iraq in 2012. He finished his PhD in Electronics from Mosul University / Iraq in 2023. His research interest in Microelectronic, IC Design, RF power amplifier design, and Intelligent Systems. He is now a lecturer in Electrical Engineering Department in Mosul university / Iraq.

**Dr. Khalid K. Mohammed** was born in (1959) in Mosul / Iraq, he received the B.Sc. degree from the University of Mosul / Electrical Engineering Department at electronic & communication 1982. He finished his M.Sc. in Electronics from Mosul University / Iraq in (1988). He finished his PhD in Electronics from Mosul University / Iraq in 2002. His research interest in Microelectronic, solar cell fabrication, power amplifier circuits, and solid-state materials. He is now a lecturer (professor) in the Electrical Engineering Department in Mosul university / Iraq, and a dean of Electronic Engineering, College/Ninevah university, Mosul, Iraq.